Int. J. Multiphase Flow Vol. 16, No. 5, pp. 819–834, 1990
Printed in Great Britain

0301-9322/90 $3.00 + 0.00
Pergamon Press/Elsevier

THE BEHAVIOR OF SOLID PARTICLES IN A VERTICAL TURBULENT BOUNDARY LAYER IN AIR†

C. B. ROGERS‡ and J. K. EATON
Mechanical Engineering Department, Stanford University, Stanford, CA 94305-3030, U.S.A.

(*Received* 23 *November* 1988; *in revised form* 5 *February* 1990)

Abstract—This paper presents the results of an experimental investigation on the response of solid particles to a zero-pressure gradient, vertical, turbulent boundary layer in air. Two different size classified glass beads, 50 and 90 μm dia (Re $\approx$ 1 and 4, respectively), were independently dispersed in the air flow with a 2% mass loading. Velocities of both the contaminant particles and the seeded air flow were measured using laser Doppler anemometry. The data show that the light particle loading had no effect on either the mean flow or the turbulence properties of the air boundary layer. The measured r.m.s. velocity fluctuations of both particle sizes nearly equaled the flow turbulence intensity in the streamwise direction but were strongly attenuated in the normal direction. This paper presents a model for predicting the mean particle behavior to within 2% and the particle r.m.s. velocities to within 50%.

Key Words: two-phase flows, particle-laden turbulent flows, turbulent boundary layer flows

INTRODUCTION

Turbulent gas flows laden with solid particles are common in both nature and technology but unfortunately only limited design tools are available for such flows. The addition of a particulate phase to the already complicated turbulent flow adds at least three additional dimensionless parameters to the description of the problem. Empiricism is difficult with such a large parameter space so design techniques must be based on basic principles. An improved understanding of the interactions between particles and turbulence is required.

The class of particle-laden flows can be broken up into two subclasses: flows with particle-induced flow modification; and flows without particle-induced flow modification. Many previous experiments have examined the former subclass where the particles affect the flow properties, without satisfactorily examining the simpler, but important, subclass of particle behavior in an unaffected turbulent flow. The interaction between the two phases in the first subclass will be a function of the particle properties and of the local particle concentration. In order to predict this local concentration, the behavior of the particles in a given fluid environment must be understood. In other words, the response of a particle cloud to its fluid surroundings can affect the behavior of the fluid, further complicating the interpretation of the measured results. The current experiments, therefore, examine the response of particles to a known turbulent fluid shear flow.

Certain criteria must be met to ensure minimal flow modification due to the particle phase. Globally, the particle mass flux must be small compared to the fluid mass flux so that the total drag force on the fluid due to the particle phase is much less than the viscous and pressure forces in the fluid. This must be true on a local scale as well, i.e. there must be no areas of high local particle mass loading. In addition, to ensure no particle-induced turbulence modification, the particle geometry must be carefully chosen. The diameter of each individual particle must be less than the size of the smallest energy-containing eddies in the flow, prohibiting the straining in the vicinity of the particle and the wake behind the particle from adding to the fluid turbulent energy. Meeting these criteria reduces the mechanisms for particle-induced flow modification.

The flow will interact with the particles through a variety of forces. (1) The flow will impose a steady drag force on the particle resulting from the fluid viscosity, the particle geometry and

†This paper supersedes Rogers, C. B. & Eaton, J. K. 1989 "Particle response and turbulence modification in a flat plate turbulent boundary layer" [in *Turbulence Modification in Dispersed Multiphase Flows* (Edited by Michaelides, E. E. & Stock, D. E.); ASME FED, Vol. 80], where preliminary results of this work were reported.

‡Present address: Department of Mechanical Engineering, Tufts University, Medford, MA 02155, U.S.A.

the particle relative velocity (the velocity of the particle in the reference frame of a fluid point). (2) In the case of an accelerating fluid, a pressure gradient across the particle will impose a further force on the particle. For the case of an accelerating particle, one must also consider the force resulting from (3) accelerating the fluid in the vicinity of the particle (the "added mass" force), and from (4) the inertial history of the accelerating particle (the "Basset history" force). Lastly, (5) other external forces, such as gravity, electrostatic forces and chemical forces must be considered. For the limiting case of the particle density being much greater than the carrier fluid density, however, the particle transport equation reduces to

$$\frac{\mathrm{d}}{\mathrm{d}t}\mathbf{v}_\mathrm{p} = \frac{\mathbf{f}_\mathrm{D}}{m_\mathrm{p}} + \boldsymbol{g}, \qquad [1]$$

where $\mathbf{v}_\mathrm{p}$ refers to the instantaneous particle velocity, m_p refers to the particle mass, $\boldsymbol{g}$ is the gravitational acceleration and $\mathbf{f}_\mathrm{D}$ denotes the drag force on the particle.

The total drag force on a particle is a function of the particle Reynolds number, the particle behavior, and the local fluid behavior. The particle Reynolds number relates the particle inertial forces to the fluid viscous forces; mathematically expressed as

$$\mathrm{Re}_\mathrm{p} = \frac{u_\mathrm{rel} d_\mathrm{p}}{\nu}, \qquad [2]$$

where u_rel and d_p refer to the particle relative velocity and diameter, respectively, and ν denotes the fluid kinematic viscosity. Small particles with small relative velocities ($\mathrm{Re}_\mathrm{p} < 0.1$) will have a particle drag proportional to the particle relative velocity (Stokes 1851):

$$\mathbf{f}_\mathrm{D} = 6\pi\mu\left(\frac{d_\mathrm{p}}{2}\right)u_\mathrm{rel}, \qquad [3]$$

where μ is the fluid viscosity. Furthermore, particles in fluid shear will experience a lift force. Saffman (1965) derived an expression for this lift force in the limit of small Re_p. Particle spin will also add to the particle drag force, both on its own (Rubinow & Keller 1961) and when coupled with fluid shear (Magnus 1855). In addition, high fluid/particle accelerations will affect the total particle drag (e.g. Odar & Hamilton 1964). Finally, fluid turbulence can decrease particle drag by accelerating the transition process on the fluid boundary layer on the particle (Torobin & Gauvin 1960). In this limit of small Re_p (< 10), small velocity gradients across particles, and large particle densities relative to the fluid density, seen in the current experiments, the total particle drag force is essentially the steady drag force, all other forces being negligible. Although many have tried to analytically estimate the magnitude of this drag for intermediate Re_p (e.g. Oseen 1910), the empirical relations of Morsi & Alexander (1972) were used in the current analysis because of their excellent agreement with experimental data.

Given an appropriate equation of motion, an individual particle's motion may be analyzed knowing the gas velocity field experienced by the particle. The average particle behavior could then be predicted by computing a representative sample of particle trajectories. Corsin & Lumley (1956) pointed out that what is needed is the particle relative velocity (the difference between the particle and fluid velocity) following a particle path rather than the one measured in the Eulerian reference frame. Since particles have more inertia than a corresponding fluid point, this particle-Lagrangian reference frame can be considerably different from the classical-Lagrangian reference frame of the fluid point, or the Eulerian reference frame of a probe. Predicting the effect of the difference between the reference frames is further complicated by the gravitational drift of the particle. Gravity will cause the particle to be constantly changing fluid neighborhoods, and therefore reacting to different turbulence than would be measured in the Eulerian reference frame or than would be seen by a fluid point in the classical-Lagrangian reference frame. This "crossing-trajectories effect" was first postulated by Yudine (1959).

The present set of experiments examines the behavior of a group of particles in a gas-phase turbulent boundary layer which is unaffected by the particle presence. The flat plate boundary layer was selected because it has been so extensively investigated in single-phase flows. The objectives of the experiment were then to measure both the mean and standard deviation of the particle velocity probability density function (pdf) and to relate these measurements to the known

gas-phase flow statistics. The particle/fluid interaction was restricted to steady particle drag by the use of particles with a high relative density and Re_p varied from 1 to 5.

RELATED EXPERIMENTAL WORK AND MODELS

This review will focus on experiments illuminating the behavior of particles in turbulent flows under conditions of relatively light mass loading. A full review of the related experimental work is presented in Rogers (1989). Most of the existing work has been restricted to nearly homogeneous core flows, pipe flows and jet flows. It is hard to reach any general conclusions based on the previous works, mainly because of the large variation in the parameter space. Uneven particle loading, particle acceleration, the direction of gravity and particle size and shape variation all contribute to variations in the measured particle statistics.

Particle-laden homogeneous and isotropic flow has been the focus of several experiments, with the main interest being in particle dispersion by turbulence. The earliest work in this area was by Soo *et al.* (1960) who examined the response of both 115 and 230 μm dia glass beads in a horizontal, nearly-isotropic, water flow. Particle velocities were measured photographically. Their results showed that the particles failed to modify the flow turbulence for mass loadings up to 6% and that the particle and flow rms velocities were the same.

Snyder & Lumley (1971) photographically tracked four different types of particles with time-constants ranging from 1 to 50 ms through a vertical homogeneous isotropic flow. Their main emphasis was on measuring classical-Lagrangian statistics by extrapolating from the small-particle results. The smaller time-constant particles tended to remain correlated over longer times, possibly a result of the crossing-trajectories effect.

Wells & Stock (1983) isolated the crossing-trajectories effect by electrostatically charging particles and then varying the magnetic field surrounding a near-isotropic core flow. By thus varying the effective gravitational drift velocity, they concluded that the crossing-trajectories effect was significant only for particles with drift velocities larger than the fluid r.m.s. velocities. Finally, they saw evidence that the particle inertia enhanced the particle dispersion where the gravitational drift retarded the dispersion. In the current experiments, the drift velocities were greater than the fluid fluctuating velocity, implying that the effect of crossing-trajectories affected the particle's behavior.

Krämer & Leuckel (1988) examined the behavior of particles in the nearly-homogeneous core flow of a pipe. They varied the turbulence scales by placing grids upstream of the particle injector. They derived an empirical relationship between the measured particle and fluid r.m.s. velocities based on the fluid time scale and the particle time-constant. Their equation was based on the results for glass beads ranging from 26 to 143 μm dia.

Several experiments of particle-laden fully-developed pipe flows have examined both the behavior of a particle cloud and the dispersion of a stream of particles. Householder & Goldschmidt (1969) present an overview of attempts which have been made to correlate turbulent diffusion to particle dispersion (Schmidt number) in both jet flows and pipe flows, showing a large variation in the experimental results. Again, the lack of knowledge about the response of a particle cloud to the fluid turbulence has restricted the interpretation of the measured statistics.

Lee & Durst (1982) examined the particle velocity profiles in a upward pipe flow for 100, 200, 400 and 800 μm glass beads. The particle relative velocity varied across the boundary layer, exceeding the flow velocity near the wall. A model was proposed, splitting the flow field into two areas: an area where the eddy scale was large compared to the particle scale, implying that the particle submitted to all fluid oscillations; and an area where the particles failed to be excited by the fluid turbulence. They do not incorporate the crossing-trajectories effect, and therefore their model was not used in the current experiments. Furthermore, the particles in the current experiments were excited by the larger-scale turbulence and ignored the smaller-scale turbulence and therefore were in the "intermediate" range of their model.

Others, such as Doig & Roper (1967), Reddy & Pei (1969), Tsuji *et al.* (1984), Boothroyd & Walton (1973) and Matsumoto *et al.* (1986), examined the particle induced fluid modification. Also, multiple experiments have examined the behavior of particles in water flows (e.g. Steimke & Dukler 1983), where particles will experience many of the forces that can be neglected in flows with large density differences between the phases.

A large experimental effort has examined the behavior of particle-laden jets, ranging from the work of Parthasarathy & Faeth (1987) and Modarress *et al.* (1982), examining particle/turbulence interaction, to the structure/concentration correlations of Longmire & Eaton (1989).

Existing models for predicting the behavior of particle-laden flows fall into three categories: (i) two-fluid models; (ii) trajectory models; and (iii) direct numerical simulations. The latter exactly simulates the behavior of particles in a model flow field.

Two-fluid models represent the particle behavior as a dilute, compressible gas. Extensive work has been done in this area by Ishii (1975), Harlow & Amsden (1975), Rizk & Elghobashi (1985) and Elghobashi & Abou-Arab (1983). The important implicit assumption of this model is that particle dispersion acts similarly to turbulent diffusion. Because of this assumption, many of the differences between a particle and a fluid point must be ignored.

Trajectory models assume a fluid field and then follow individual particles through that field. The "particle source in cell" technique of Crowe & Pratt (1972) first solves for the fluid phase, then uses an appropriate transport equation, taking all the necessary terms into account, to predict the particle motion. The method then finds a new solution for the fluid phase based on the updated particle position. This method is iterated until the routine converges on a solution for both the particle and the fluid field. Although this method works well for the mean statistics, it cannot imitate turbulent dispersion. Others have examined a Monte-Carlo type method (e.g. Gosman & Ioannides 1981) where the fluid turbulence is assumed to be random. Chen & Crowe (1984) showed that although this method worked well for isotropic flows, it was unable to handle non-isotropic flows.

In general, most of these models rely on some method for estimating the fluid properties along the particle path. The method most commonly chosen is to assume that the particles tend to follow a fluid point and therefore use a κ–ϵ classical-Lagrangian time-constant to relate the Eulerian and Lagrangian statistics. The particles in the current experiments had a substantial gravitational drift velocity, inhibiting the use of descriptors for a fluid point as descriptors for a single particle.

Lastly, direct numerical simulations of particle-laden isotropic and homogeneous flows have led to increased insight in the interaction between particles and their surrounding fluid. Maxey & Riley (1983) simulated the behavior of individual particles in a random flow field and saw that particles tended to collect in areas of high strain and low vorticity. Squires & Eaton (1989) saw similar behavior in direct simulations of homogeneous/isotropic flows.

EXPERIMENTAL TECHNIQUES

The present experiments were performed in a blower-driven, two-dimensional, vertical turbulent boundary-layer wind-tunnel. The flow went vertically upwards and was uniformly loaded with particles. Figure 1 shows the full schematic of the tunnel. The air was driven by a 1 hp blower through extensive flow conditioning before entraining particles in the particle feeder. The flow conditioning consisted of two diffusers with four large grids and a right-angle section directing the flow upward. The flow then passed through the particle feeding section and through a set of grids to enhance particle/fluid mixing. After the grids, the flow passed through a 3:1 contraction and then a 3.8 cm thick hexagonal honeycomb (0.48 cm cell size) at the test section entrance. The honeycomb was installed to keep the particle distribution uniform; without it the contraction shape would cause all the particles to migrate toward the tunnel centerline. The test section was a rectangular channel, 7.6 × 46 cm, and 100 cm tall. All of the test section walls were Plexiglas for optical access for laser Doppler anemometry. The boundary layer was tripped upon entry to the test section by a 0.16 cm plastic strip which spanned the test wall. The particles were then recovered after the test section using a cyclone separator.

It was imperative to have a very controlled, evenly loaded, uniform second phase. For this reason we designed a unique particle feeding system (figure 2). Two belts crossed the wind-tunnel at four spanwise locations. Each belt had 50 1.3-cm tall aluminum buckets attached to it. Each bucket had a large entrance (10 mm dia) but a small exit area (1.5 mm dia) so that the buckets could be rapidly filled on either side of the tunnel and would drain at a constant rate as they moved across the tunnel. Figure 3 is a schematic of a single belt showing the feeding method. The particles fall out of the bottom of the bucket to be entrained by the flow and swept upward into the test section. The grids,

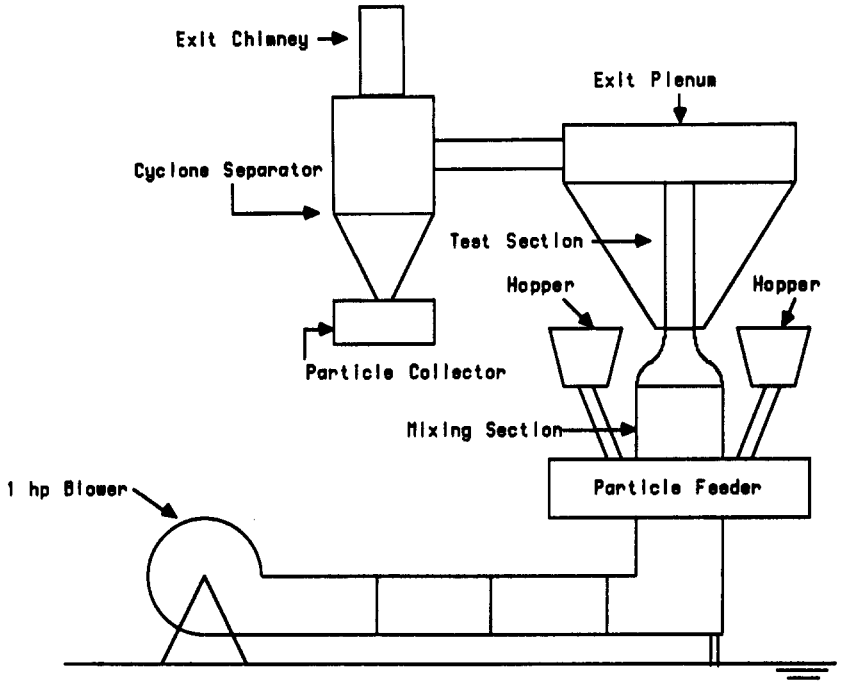

Figure 1. Wind-tunnel schematic.

the contraction and the honeycomb downstream all ensured further loading uniformity. The uniformity was checked both visually with a laser sheet, and quantitatively by the LDA. The particle concentration varied $<5\%$ across the boundary layer. This measurement resulted from comparing the normalized average data rate for the particle phase at all longitudinal positions to the normalized particle mean velocity.

Two different size glass beads were used for the particle phase in the present set of experiments and are described in table 1. All particles were commercially sized to ensure a 10 μm window in the particle diameters. Figure 4 shows the resulting distribution in the particle diameters. Talcum powder was used as a flow tracer and was injected with an airbrush upstream of the blower.

The LDA system was a low-power, single-component, forward-scattering system. A 4 mW He–Ne laser, used in conjunction with a beamsplitter, supplied the two beams spaced 50 mm apart. The beams were focused using a 480.5 mm focal length lens. The resulting measuring volume was 0.5 mm dia, containing approx. 80 fringes; 6.1 μm apart. This relatively large diameter inhibited accurate velocity measurements closer than 4 mm ($y^+ = 100$) from the wall. By rotating the optics and inserting a Bragg Cell (1 MHz shift), negative velocities could be accommodated in the normal direction. Collection optics were used in the on-axis, forward-scatter configuration. The signal from the photomultiplier tube was processed using a TSI Model 1980B counter processor interfaced to an IBM PC.

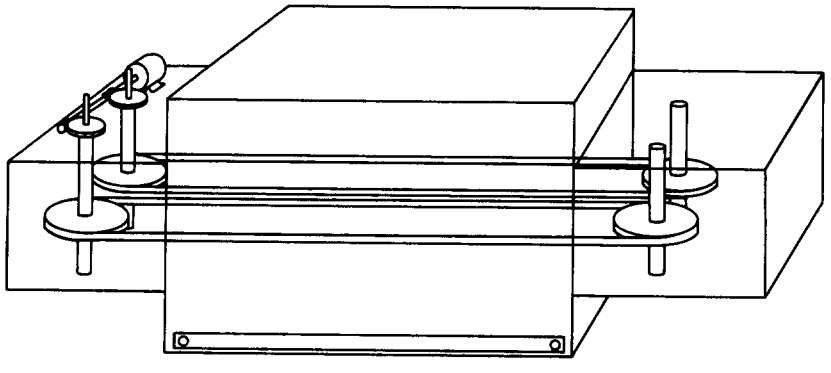

Figure 2. Particle feeder: full schematic.

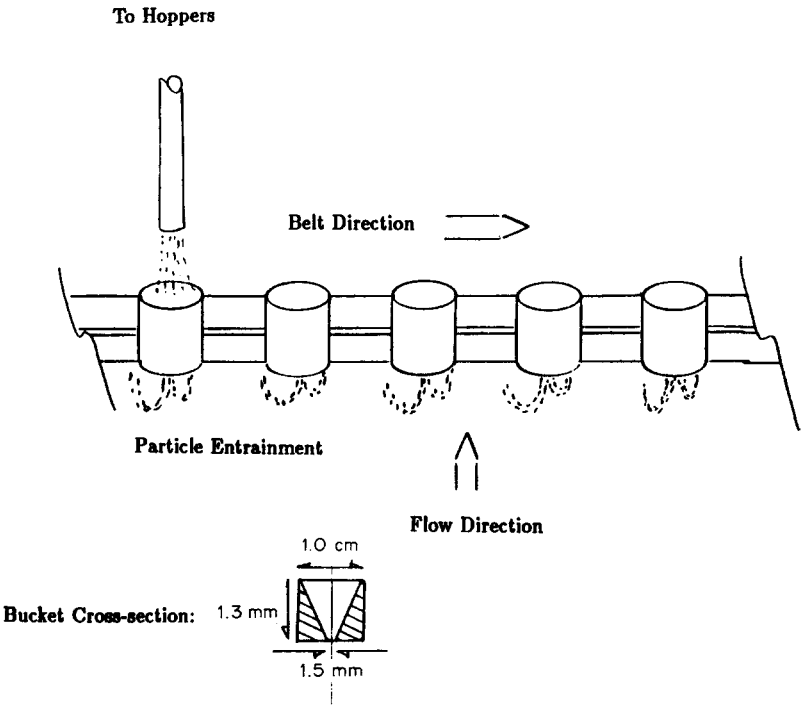

Figure 3. Particle feeder: single belt.

The diameter difference between the particles and the flow seed was large enough to use a discrimination scheme based on the intensity of the scattered light. The discrimination setting was reset before every run by examining the probability density functions of the velocity of the air flow both with and without particles. Since the particle loading was low enough that the gas phase remained unchanged in the presence of the particles, all variations in the probability density function of the fluid would result from particle contamination, i.e. signals from particles being interpreted as flow tracers. Conversely, there was no measurable contamination of the particle statistics by the flow tracers. The preamplifier gain was reduced so that the flow tracers did not provide sufficient strength to trigger the processing electronics. Figure 5 demonstrates the effect of particles on the flow probability density function and shows that particle contamination effects are negligible.

Flow power spectra were also calculated using the LDA. The conventional method of finding spectra using a fast Fourier transform of a periodically sampled velocity record is not feasible with an LDA in air flow because of the random intersample time. A multitude of methods for computing power spectra from LDA data have been presented in the literature (e.g. Adrian 1987). In particular, the straightforward method of Gaster & Roberts (1977) was used. The gas-phase power spectra were computed by taking the direct Fourier transform of the calculated velocity

Table 1. Description of experimental parameters for particles

	Particle dia (μm)	
	50	90
Material	Glass	Glass
Diameter range (μm)	45–55	85–95
Density (kg/m^3)	2500	2500
Mass loading (g/s)	5	5
Mass fraction	0.02	0.02
Volume loading (cm^3/s)	2	2
Volume fraction	10^{-5}	10^{-5}
Stokes time constant (s)	0.019	0.0625
Correction factor	1.1	1.4
Corrected time constant (s)	0.018	0.044
Re_p range	1.0–1.2	2.2–4.5

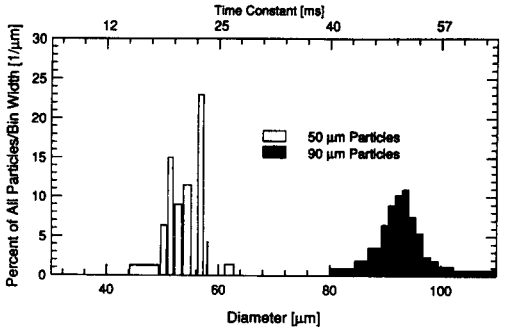

Figure 4. Diameter distribution of glass particles.

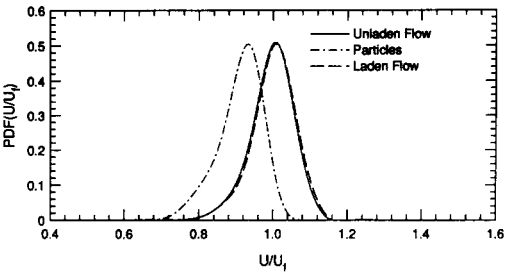

Figure 5. Effect of particles on flow velocity PDF 10 mm from the wall.

autocorrelation. The autocorrelation was formed by dividing the time-axis into 1000 bins, each 0.5 ms long. To ensure statistically stable autocorrelations, 50,000 points were taken. Gaster & Roberts showed that the Poisson distribution of the intersample time alleviated all aliasing problems. Figure 6 compares power spectra taken by a hot wire and an LDA. The agreement is within the measurement uncertainty.

The measurement uncertainty in these experiments, for a 95% confidence level, is 3% for the unladen gas-phase mean and fluctuating measurements. The uncertainty results from errors in particle discrimination, and the limitations of a finite data sample. All errors due to velocity bias are $<1\%$ for the given fluid turbulence levels. Errors in the particle statistics are slightly higher. Variations in particle history, particle shapes and particle diameters increase the uncertainty to 5% in the mean. It can be shown that a 10 μm variation in the particle diameter can result in up to a 30% increase in the measured r.m.s. particle velocity (Rogers 1989).

RESULTS

The main results presented in this paper fall into two categories: mean and fluctuating velocity profiles for the gas and particle phases. Results are presented at two axial stations: $X = 55$ and 85 cm above the boundary layer trip. The fluid boundary layer characteristics are listed in table 2. In the following paragraphs, "unladen flow" will refer to measurements made of the gas phase in the absence of particles and "laden flow" will refer to measurements made of the gas phase in the presence of particles.

Table 2. Fluid parameters [dissipation from Murlis *et al.* (1982): $Re_\theta = 1089$]

Flow parameters	$X = 55$ cm	δ_{99}	20 mm
		Freestream velocity	8.0 m/s
		Displacement thickness (δ^*)	3.0 mm
		Momentum thickness (θ)	2.1 mm
		Shape factor (H)	1.4
		Re_{δ^*}	1550
		Re_θ	1090
		U_τ	0.38 m/s
		Skin friction coefficient ($C_f/2$)	0.0022
	$X = 85$ cm	δ_{99}	24 mm
		Freestream velocity	8.2 m/s
		Displacement thickness (δ^*)	3.8 mm
		Momentum thickness (θ)	2.6 mm
		Shape factor (H)	1.4
		Re_{δ^*}	2020
		Re_θ	1410
		U_τ	0.37 m/s
		Skin friction coefficient ($C_f/2$)	0.0020
Flow scales	$X = 55$ cm, $y^+ = 300$	Dissipation	5.0 m/s^2
		Kolmogorov length scale	0.16 mm
		Integral scale (streamwise)	7.3 mm
		Integral scale (normal)	3.8 mm

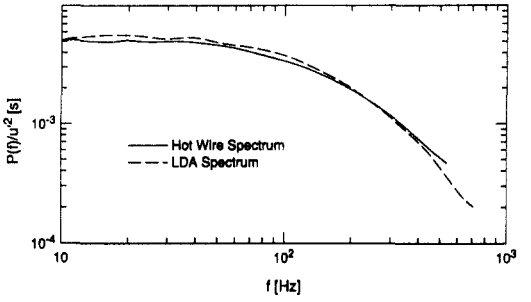

Figure 6. Spectral check: flow power spectra. $X = 55$ cm, $y^+ = 300$.

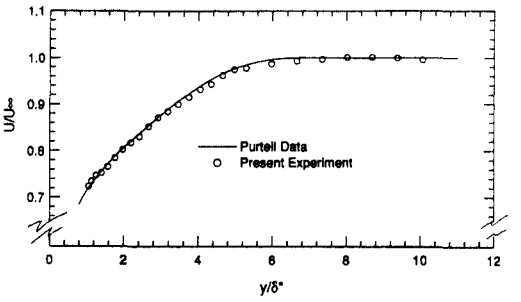

Figure 7. Qualification: comparison of mean velocity profiles.

A hot-wire anemometer was used to qualify the tunnel. First, the comparison between the hot-wire and LDA measurements ensured that the talcum flow tracer was accurately following a fluid point. Second, the two-dimensional nature of the flow in the test section was documented by making spanwise traverses across the flow. The mean velocity was found to vary $<2\%$ across the span of the boundary layer. Last, the velocity profiles and calculated wall-friction coefficients were compared to the data of Purtell *et al.* (1981). The agreement in the mean and r.m.s. velocity measurements was better than 2%, except for the slightly larger freestream turbulence in the present results due to the honeycomb at the test section entrance. Figures 7 and 8 compare the measured velocity statistics of Purtell *et al.* (1981) to the present experiment. Figure 9 compares the wall-friction coefficient distribution compiled by Purtell *et al.* to those calculated at both downstream locations in the present experiments. The agreement is within 5%.

Particle response to mean fluid velocity

Before examining the behavior of the particles in a gas boundary layer, one must ensure that the particles are not affecting the behavior of the boundary layer. Figures 10(a, b) show the boundary layer profiles, both with and without particles. The agreement is better than the quoted 3% uncertainty, implying that the effect of the particle phase on the behavior of the fluid phase was negligible.

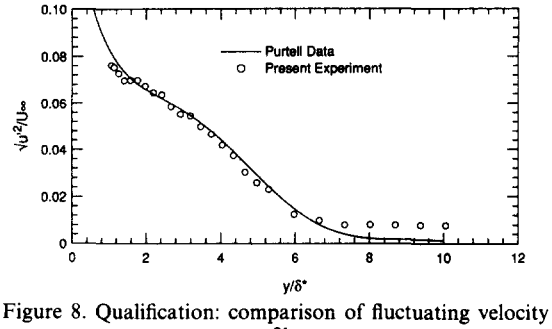

Figure 8. Qualification: comparison of fluctuating velocity profiles.

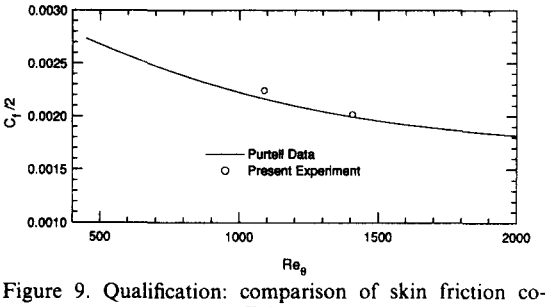

Figure 9. Qualification: comparison of skin friction coefficients.

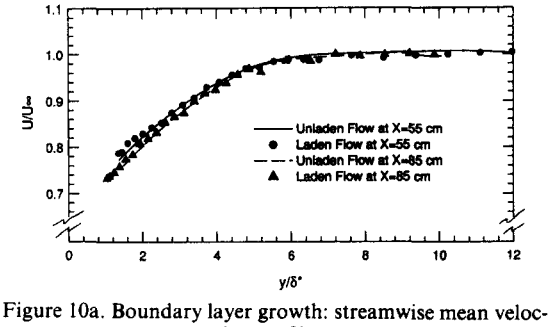

Figure 10a. Boundary layer growth: streamwise mean velocity profiles.

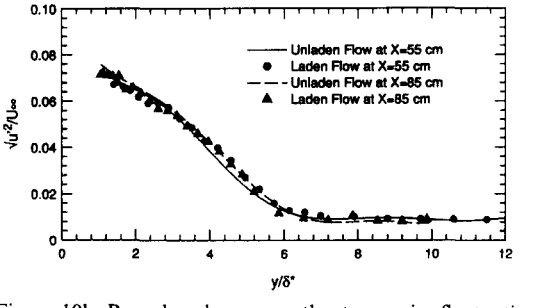

Figure 10b. Boundary layer growth: streamwise fluctuating velocity profiles.

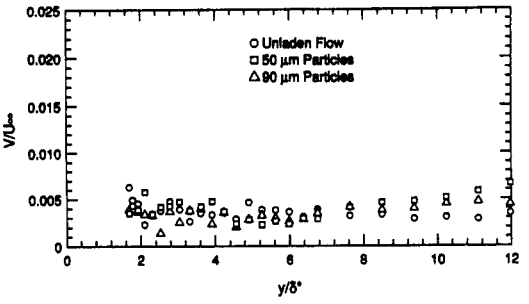

Figure 11. Normal mean velocity profiles. $X = 55$ cm.

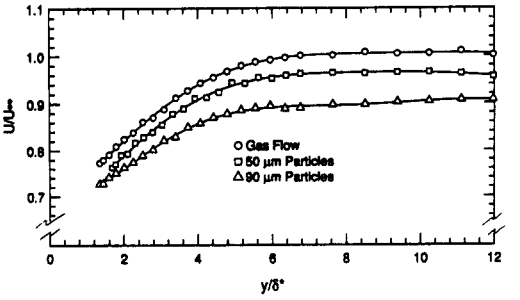

Figure 12. Streamwise mean velocity profiles. $X = 55$ cm.

Mean particle and fluid velocity components normal to the wall were measured (figure 11) to ensure no normal particle migration. Figure 11 shows that the honeycomb at the contraction exit was successsful in eliminating the normal velocity component of the particles resulting from the contraction geometry. The non-zero values result from slight beam misalignment.

The particle mean velocity profile shown in figure 12 was similar in shape to the fluid velocity profile, but at a lower mean velocity due to gravity. As expected, the relative velocity for larger particles is greater. Comparison of the particle and flow velocity profiles shows a small variation in the particle relative velocity across the boundary layer. Some authors have attributed similar variations to variations in the particle drag coefficient caused by fluid turbulence. In these experiments, however, there is no increase in particle drag due to turbulence but rather this variation is a direct result of particle acceleration. Particles closer to the wall are convected upward by a slower velocity fluid than those in the freestream. Therefore, the particle velocities measured close to the wall will be those of particles whose residence time (i.e. time in the test section) is greater than corresponding particles in the freestream. Thus, particles closer to the wall will be closer to their asymptotic velocity than particles in the freestream. The particle asymptotic velocity is the particle terminal velocity measured in an Eulerian reference frame, i.e. the velocity of a particle where drag forces and gravitational forces are equal and opposite. At the limit of long residence times, the particule relative velocity will be constant across the boundary layer.

In order to check the hypothesis that the particle relative velocity variation across the boundary layer is solely a function of particle acceleration, a model for estimating the particle velocity from the fluid velocity was developed. The assumptions were: (1) the particle drag force varies linearly with the particle relative velocity; (2) all particles have the same initial velocity, entering the test section; (3) the fluid axial acceleration is much smaller than the particle axial acceleration; (4) the particle is accelerated by a constant fluid speed; (5) the normal component of the particle fluctuations is small compared to the particle mean velocity; and (6) the only external body force on the particles is the gravitational force.

Based on Stokes' analysis for small Re_p (<0.1), the particle transport equation can be written as

$$\frac{d}{dt}\mathbf{v}_p = \alpha \mathbf{u}_{rel} + \boldsymbol{g}, \qquad [4]$$

where $\mathbf{v}_p$ is the particle velocity, $\boldsymbol{g}$ is the gravitational acceleration and α is a constant of proportionality. In the limit of small Re_p (<0.1), α will approach the reciprocal of the Stokes time-constant,

$$\tau_{Stokes} = \frac{\rho_p d_p^2}{18\mu}, \qquad [5]$$

where ρ_p and d_p are the particle density and diameter, respectively, and μ refers to the fluid viscosity. The Stokes solution is not valid for the Re_p in the current experiments ($1 < Re_p < 5$), and therefore an empirically derived time-constant was used and the small non-linear drag terms were neglected. The empirical time-constant was defined as

$$\tau = \frac{1}{\alpha} = \frac{u_{term}}{g}, \qquad [6]$$

where u_{term} is the particle terminal velocity. It is implicitly assumed that the mean particle direction is in the streamwise direction, implying that only the streamwise components of the particle and fluid velocities are important. The plot of particle normal velocities, figure 11, substantiates this assumption. Equation [6] results from evaluating the particle transport equation [4] at the particle asymptotic velocity (i.e. $d\mathbf{v}_p/dt = 0$). The particle terminal velocity was estimated from the empirical relationship derived by Morsi & Alexander (1972) relating Re_p and the particle drag force.

The particle velocity as a function of particle position can be derived from the particle transport equation [4]. Integrating [4] twice will give an expression for the position of a particle, x_p, assuming a particle initial velocity of v_0. Combining this equation, using $x_p = 0$ as an initial condition, with the equation for the particle velocity (the integral of [4]), gives the relationship between the particle position and velocity of

$$\mathbf{x}_p(\mathbf{v}_p) = \tau v_a \ln\left(\frac{\Delta v}{\Delta v - \delta v}\right) - \tau \delta v, \qquad [7]$$

where v_a is the particle asymptotic velocity (i.e. $u_f - g\tau$), Δv is the difference between the particle asymptotic velocity and its initial velocity (i.e. $v_a - v_0$) and δv is the difference between the present particle velocity and its initial velocity [i.e. $v_p(t) - v_0$]. Invoking the assumption that normal particle movement is small [i.e. assumption (4)], one can assume that x_p can be estimated by the distance from the test section entrance, X. The initial particle velocity, v_0, was determined by evaluating [7] at one axial position in the freestream with a known particle relative velocity. Using this equation, with the corrected time-constant, for any given distance into the test section (e.g. $X = 55$ or 85 cm), the estimated particle velocity could be determined iteratively, given the local flow velocity. The difference between the measured and estimated particle velocity profiles at $X = 55$ cm in figure 13 is $<2\%$. This excellent agreement implies that in these experiments, the variation in particle relative velocity across the boundary layer was a function of only the particle acceleration.

Rather than determine a new v_0 for $X = 85$ cm, a more rigorous approach was used. The growth of the boundary layer could be accounted for by assuming a constant du_f/dt due to the increase in the displacement thickness. Assumption (4) must be generalized to assume that the particle has only been accelerated by the thin column of fluid starting at a given velocity at $X = 55$ cm and experiencing a constant fluid acceleration. The particle transport equation becomes

$$\frac{d}{dt}\mathbf{v}_p(t) = \frac{1}{\tau}\left[u_{55cm} + \frac{du}{dt}t - \mathbf{v}_p(t)\right] - \boldsymbol{g}, \qquad [8]$$

where

$$u_{85cm} = u_{85cm} + \frac{du}{dt}t$$

and refers to the fluid velocity at the $X = 85$ cm station. Repeating the previous analysis, and taking du_f/dt to be constant, the result is identical to [7] with an effective decrease in the particle asymptotic velocity:

$$\tilde{v}_a = v_a - \tau\frac{d}{dt}u_f, \qquad [9]$$

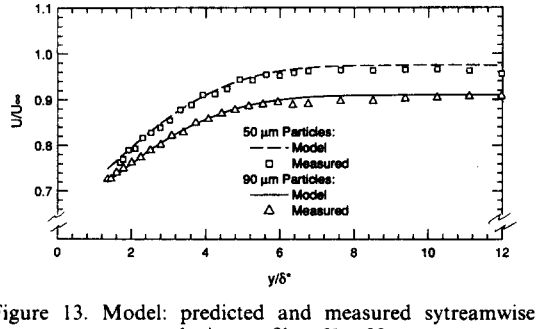

Figure 13. Model: predicted and measured sytreamwise mean velocity profiles. $X = 55$ cm.

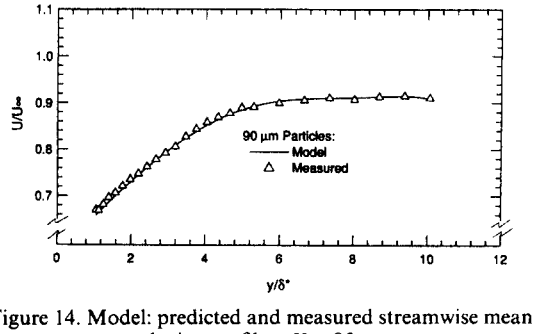

Figure 14. Model: predicted and measured streamwise mean velocity profiles. $X = 85$ cm.

where $\tilde{v}_a$ now refers to the particle asymptotic velocity at $X = 85$ cm. The constant flow acceleration was estimated by

$$\frac{d}{dt}u_f = -\frac{u^3}{u_1 A_1}\frac{\Delta A}{\Delta X}, \qquad [10]$$

from the conservation of mass, where A_1 and u_1 are the cross-sectional area (minus the displacement thickness) and the flow freestream velocity, respectively, at an arbitrary point in the test section. Both the vertical distance traveled by the particle and the change in tunnel cross-sectional area are denoted by ΔX and ΔA, respectively. Figure 14 clearly demonstrates that this small correction is quite accurate for very slight flow accelerations.

In conclusion, the excellent agreement between the model predictions and the empirical data demonstrates that for Re_p of up to 5, a linear drag law can be used for the prediction of particle velocities as long as a corrected particle time-constant is used. This implies that, in the limit of small fluid accelerations, the crossing-trajectories effect has a negligible effect on the mean particle velocity. That is, the fluid properties along a particle path are relatively constant in the mean. No hypothetical increase in particle drag due to the presence of the wall (e.g. Matsumoto *et al.* 1986) was seen in this experiment.

Particle response to fluid turbulence

The meanings of the measured r.m.s. particle velocity fluctuations are different from the corresponding single-phase fluid turbulence. Where fluid turbulence intensities portray the total turbulent kinetic energy of eddies in the fluid, the particle velocity fluctuations are a measure of the ability of a particle to respond to those eddies. A particle with a large time-constant, as compared with the fluid time-constant, will be unable to respond to the fluid turbulence and therefore should have no measurable r.m.s. velocity fluctuations. Equally, extremely small time-constant particles, e.g. the talcum powder, will have very little inertia and will have the same r.m.s. velocity fluctuations as the surrounding flow. A good measure for the ability of a particle to respond to fluid turbulence would be the Stokes number; the ratio of the particle time-constant to some characteristic fluid time scale. The Stokes number used in the current experiments was of the order of unity.

Furthermore, all variations in the particle diameter, variations in the history of fluid neighborhoods experienced by a particle and variations in particle inertia will be measured as an increase in the particle r.m.s. velocity. A slightly smaller particle, say 85 μm dia, will have a lower asymptotic velocity than the corresponding slightly larger, 95 μm dia, particle. These variations in particle diameter can increase the measured particle r.m.s. velocity by as much as 30% for the particles in the present experiments (Rogers 1989).

The standard deviation of the particle velocities are shown in figure 15 for the streamwise component and in figure 16 for the normal component. The particle velocity fluctuations are actually slightly greater than the corresponding fluid turbulence intensity in the streamwise direction for both the 50 and 90 μm dia particles. The standard deviation of the particle normal velocities shows the expected damped response, the damping being greater for the larger particles with longer time-constants. The differences in the apparent particle response between the

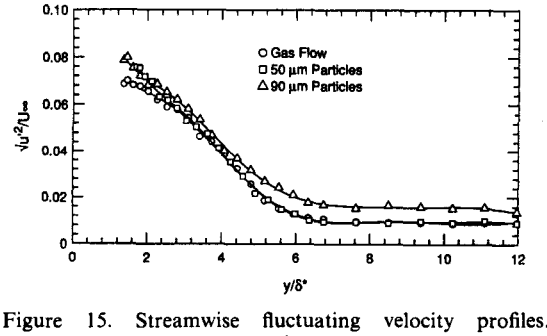

Figure 15. Streamwise fluctuating velocity profiles. $X = 55$ cm.

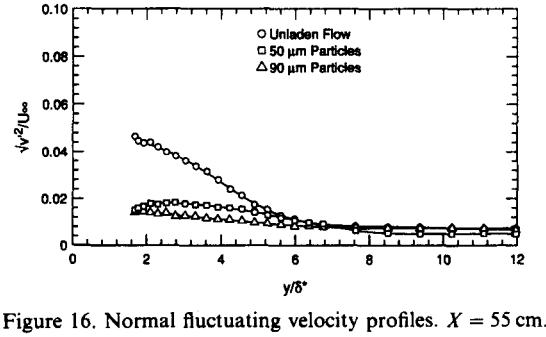

Figure 16. Normal fluctuating velocity profiles. $X = 55$ cm.

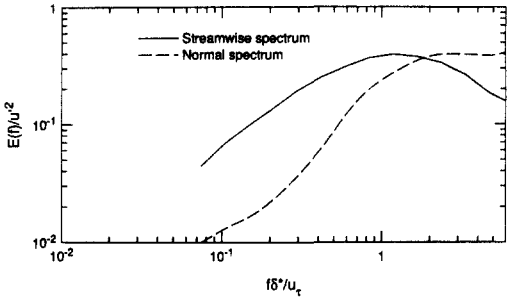

Figure 17. Flow energy spectra. $X = 55$ cm, $y^+ = 300$.

streamwise and normal directions can be at least partially explained by examining the typical flow energy spectra shown in figure 17. The bulk of the energy in the normal component occurs at a significantly higher frequency than the streamwise component. Therefore, one would expect the particles to respond to a smaller fraction of the fluid velocity fluctuations in the normal direction.

The argument above cannot fully explain the fact that the particle r.m.s. velocity in the streamwise direction is nearly the same as the corresponding streamwise fluid turbulence intensity. The inverse of the particle time-constant, in the dimensionless scale of figure 17, is 0.43 for the 50 μm particles and 0.16 for the 90 μm particles. Therefore, after examining figure 17, one would expect the particle response to be substantially attenuated relative to the flow turbulence intensity. Additional effects which act to increase the measured r.m.s. particle velocity will be discussed after the following presentation of Csanady's model.

In order to model the response of the particles to the fluid turbulence, Csanady (1963) derived a relationship between the fluid and particle power spectra. He assumed that: (1) the particle and flow velocities were periodic in time; (2) the particle and fluid fluctuated in phase; (3) the particle drag was a linear function of the particle relative velocity; and (4) a particle was always excited by identical fluid turbulence. He derived the relationship between the particle and fluid power spectra to be

$$Q_p(v) = \frac{1}{1 + 4\pi^2 v^2 \tau^2} Q_f(v), \qquad [11]$$

where $Q_p(v)$ and $Q_f(v)$ are the particle and fluid power spectra, respectively, and v is the measured frequency.

The problem with Csanady's derivation is that it relates the particle power spectrum to the fluid spectrum along with a particle path. He then assumed that the fluid turbulence experienced by a particle along the particle path would be the same as the fluid turbulence measured by a stationary probe. Directly applying [11] to spectra taken at a few points in the boundary layer shows poor agreement with the measured results (table 3). That is, the crossing-trajectories effect is not negligible in determining the response of the particle.

A method is required to translate the fluid power spectrum measured in the Eulerian reference frame to a corresponding power spectrum in the particle-Lagrangian reference frame. A fluid eddy will pass by a stationary probe substantially faster than it passes by a particle convecting with the

Table 3. Results of Csanady's model without corrected frequency.

Velocity	X location (cm)	Y location (mm)	50 μm predicted	50 μm measured	90 μm predicted	90 μm measured
Streamwise	55	4	0.29	1.2	0.15	1.1
		13	0.25	0.98	0.14	1.1
		38	0.30	0.92	0.16	1.6
	85	4			0.15	1.1
		13			0.14	1.0
		38			0.18	1.2
Normal	55	6	0.08	0.39	0.05	0.33
		13	0.09	0.73	0.04	0.48
		38	0.07	0.63	0.04	0.80

All values are ratios of particle to flow r.m.s. velocities $\left(\frac{\sqrt{u_p'^2}}{\sqrt{u_f'^2}}\right)$.

flow. Therefore, a frequency measured in the Eulerian sense will be larger than the corresponding frequency measured in a particle-Lagrangian sense. In order to quantify the relationship between the two spectra, consider a very simple description of frozen turbulence, i.e. a velocity field frozen in space, moving past both a measurement probe and a moving particle. A frequency will be measured by the Eulerian probe as this eddy passes by with a velocity, u_f, of

$$\nu_{\text{Eulerian}} = \frac{u_f}{l_e}, \qquad [12]$$

where l_e is the characteristic eddy length. The same eddy passing by the particle would have a frequency of

$$\nu_{\text{particle}} = \frac{u_{\text{rel}}}{l_e}. \qquad [13]$$

Combining [12] and [13] gives the relationship between the two reference frames as being

$$\nu_{\text{particle}} = \frac{u_{\text{rel}}}{u_f} \nu_{\text{Eulerian}}. \qquad [14]$$

Using this frequency stretching term in [14] gives substantially better results (table 4). The agreement in the measured and predicted particle r.m.s. velocities are within the quoted experimental uncertainty for the smaller time-constant particles. The 90 μm particles, however, still have greater fluctuations than predicted.

The increased error in the r.m.s. velocity predictions for the larger time-constant particles partially results from the increase in particle inertia. The larger particles have a larger mass and therefore the inertial effects on the particle behavior will be greater. The correction factor only accounts for the change of fluid neighborhood due to gravitational drift. As the particle inertia increases, however, the variation in the fluid neighborhood around a particle resulting from particle inertia will have a larger effect on the particle r.m.s. fluctuations. This effect will be more prominent in the r.m.s. velocity for the larger particles, decreasing the accuracy of the model.

The frozen turbulence assumption can be checked by comparing the time it takes a particle to traverse an eddy to the eddy turnover time. Using the κ–ϵ estimation of an isotropic eddy turnover time,

$$t_e = \frac{l_e}{\mathbf{u}_f'}, \qquad [15]$$

with

$$l_e = 0.3 \frac{\kappa^{3/2}}{\epsilon}. \qquad [16]$$

one can estimate the "lifetime" of an eddy in the gas flow of the present experiments. Comparing this time, then, to the time it takes a particle to traverse the eddy,

$$t_r = \frac{l_e}{\mathbf{u}_f - \mathbf{v}_p}, \qquad [17]$$

Table 4. Results of Csanady's model with corrected frequency.

Velocity	X location (cm)	Y location (mm)	50 μm predicted	50 μm measured	90 μm predicted	90 μm measured
Streamwise	55	4	0.79	1.2	0.56	1.1
		13	0.82	0.98	0.48	1.1
		38	0.85	0.92	0.56	1.6
	85	4			0.57	1.1
		13			0.54	1.0
		38			0.60	1.2
Normal	55	6	0.36	0.39	0.20	0.33
		13	0.58	0.73	0.24	0.48
		38	0.38	0.63	0.15	0.80

All values are ratios of particle to flow r.m.s. velocities $\left(\frac{\sqrt{u_p'^2}}{\sqrt{u_f'^2}}\right)$.

indicates that the eddies in the flow field decay almost as rapidly as particles traverse them. The ratio of the two time scales,

$$\frac{t_r}{t_e} = \frac{|\mathbf{u}'|}{\mathbf{u}_{rel}}, \qquad [18]$$

governs the validity of the assumption. Taking, for example, the location in the boundary layer at $y^+ = 300$ and $X = 55$ cm, the particle residence time for the 90 μm particles is about 40% of the isotropic eddy lifetime. The particle residence time for the 50 μm particles is about equal to the eddy lifetime (about 6 ms). It should be noted here that the estimates for ϵ came from the experimental data of Murlis *et al.* (1982) (see table 2) and κ was estimated from the measured u' and v' values. Thus, the frozen turbulence assumption is far from accurate for the particles used in the current experiments, yet the results from this assumption work well for the smaller time-constant particles. It would therefore appear that this modification of the Csanady model, with the appropriate stretching in frequency space, is restricted by particle inertia, rather than by eddy dissipation.

Thus, particles with a significant relative velocity will be excited by a different energy spectrum than is measured in the Eulerian reference frame. For Re_p close to 1, the inertial effects are small and the particle relative velocity can be taken into account by a simple correction term. As Re_p increases, the particle inertial effects increase the measured particle r.m.s. velocity.

CONCLUSION

The results from the set of experiments described above demonstrated three important points about a lightly loaded, two-phase boundary layer. First, the evenly loaded (2% by mass) particle phase has no effect on the behavior of the gas-phase boundary layer. Second, the mean velocity profiles can be predicted by assuming a linear relationship between the particle drag and the particle relative velocity for particles up to $Re_p = 5$ simply by adjusting the particle time-constant to account for the difference between Stokes drag and the particle's actual drag. Third, the particle r.m.s. velocities can be predicted for Re_p values of about 1 to within 20%. As Re_p increased, the prediction method failed. The proposed model does predict the directional attenuation of the particle r.m.s. velocity that was seen in the current experiments.

This paper has presented an accurate method for predicting the mean particle transport in a vertical, turbulent boundary layer. It has also shown that non-Stokesian particles have substantially greater r.m.s. velocities than previously predicted, although the data reflect the trends predicted by the models.

Acknowledgement—The authors are grateful for the sponsorship from the National Science Foundation (Grant No. MEA-83-51417).

REFERENCES

ADRIAN, R. J. & YAO, C. S. 1987 Power spectra of fluid velocities measured by laser Doppler velocimetry. *Expts Fluids* **5,** 17–28.

ARNASON, G. 1982 Measurement of particle dispersion on turbulent pipe flow. Ph.D. Thesis, Washington State Univ., Pullman, Wash.

BAXTER, L. L. & SMITH, P. J. 1988 Turbulent dispersion of particles, Brigham Young Univ., Provo, Utah.

BOOTHROYD, R. G. & WALTON, P. J. 1973 Fully developed turbulent boundary-layer flow of a fine solid–particle gaseous suspension. *Ind. Engng Chem. Fundam.* **12,** 75–82.

CHEN, P. P. & CROWE, C. T. 1984 On the Monte-Carlo method for modeling particle dispersion in turbulence. In *Proc. Energy Sources Technology Conf.*, New Orleans, La, pp. 37–41.

CORRSIN, S. & LUMLEY, J. 1956 On the equation of motion for a particle in turbulent fluid. *Appl. scient. Res.* **A6,** 114–116.

CROWE, C. T. & PRATT, D. T. 1972 Two-dimensional gas–particle flow. Presented at the *1972 Heat Transfer and Fluid Mechanics Institute*, Stanford Univ., Calif.

CSANADY, G. T. 1963 Turbulent diffusion of heavy particles in the atmosphere. *J. atmos. Sci.* **20,** 201–208.

DOIG, I. D. & ROPER, G. H. 1967 Air velocity profiles in the presence of currently transported particles. *Ind. Engng Chem. Fundam.* **6,** 247–256.

ELGHOBASHI, S. E. & ABOU-ARAB, T. 1983 A two-equation turbulence model for two-phase flows. *Phys. Fluids* **26,** 931–938.

GASTER, M. & ROBERTS, J. B. 1975 Spectral analysis of randomly sampled signals. *J. Inst. Math. Applic.* **15,** 195–216.

GASTER, M. & ROBERTS, J. B. 1977 The spectral analysis of randomly sampled records by direct transform. *Proc. R. Soc. Lond.* **A354,** 27–58.

GOSMAN, A. D. & IOANNIDES, E. 1981 Aspects of computer simulation of liquid-fueled combustors. In *Proc. 19th Aerospace Science Mtg*, St Louis, Mo., AIAA Paper 81-0323.

HARLOW, F. & AMSDEN, A. 1975 Numerical calculation of multiphase fluid flow. *J. comput. Phys.* **17,** 19–52.

HOUSEHOLDER, M. K. & GOLDSCHMIDT, V. W. 1969 Turbulent diffusion and Schmidt number of particles. *ASCE Jl Engng Mech. Div.* **EM6,** 1345–1367.

ISHII, M. 1975 *Thermo-fluid Dynamic Theory of Two-phase Flow.* Eyrolles, Paris, France.

KRÄMER, M. & LEUCKEL, W. 1988 Experimental and theoretical investigations on the behavior of solid particle motion in turbulent gaseous flows. Presented at the *Lisbon LDA Symp.*, Lisbon, Portugal.

LEE, S. L. & DURST, F. 1982 On the motion of particles in turbulent duct flows. *Int. J. Multiphase Flow* **8,** 125–146.

LONGMIRE, E. K. & EATON, J. K. 1989 Structure and control of a particle-laden round jet. Presented at *Fluids Engineering and Science: the U.S.–Korea Joint Semin.*, Seoul, Korea.

MAGNUS, G. 1855 Hydraulic investigations. *Pogg. Annln Phys.* **95,** 1–59.

MATSUMOTO, S., HARAKAWA, H., SUZUKI, M. & OHTANI, S. 1986 Solid particle velocity in vertical gaseous suspension flows. *Int. J. Multiphase Flow* **12,** 445–458.

MAXEY, M. R. & RILEY, J. J. 1983 Equation of motion for a small rigid sphere in a non-uniform flow. *Phys. Fluids* **26,** 883–889.

MODARRESS, D., WUERER, J. & ELGHOBASHI, S. 1982 An experimental study of a turbulent round two-phase jet. In *Proc. AIAA/ASME 3rd Joint Thermophysics, Fluids, Plasma, and Heat Transfer Conf.*, St Louis, Mo., Paper AIAA-82-0964.

MORSI, S. A. & ALEXANDER, A. J. 1972 An investigation of particle trajectories in two-phase flow systems. *J. Fluid Mech.* **55,** 193–208.

MURLIS, J., TSAI, H. M. & BRADSHAW, P. 1982 The structure of turbulent boundary layers at low Reynolds numbers. *J. Fluid Mech.* **122,** 13–56.

ODAR, F. & HAMILTON, W. S. 1964 Forces on a sphere accelerating in a viscous fluid. *J. Fluid Mech.* **10,** 302–314.

OSEEN, C. W. 1910 Über die Stokes'she Formel und über eine verwandte Aufgabe in der Hydrodynamik. *Ark. Mat. Astr. Fys.* **6,** 29.

PARTHASARATHY, R. N. & FAETH, G. M. 1987 Structure of particle-laden turbulent water jets in still water. *Int. J. Multiphase Flow* **13,** 699–716.

PURTELL, L. P., KLEBANOFF, P. S. & BUCKLEY, F. T. 1981 Turbulent boundary layer at low Reynolds number. *Phys. Fluids* **24,** 802–806.

REDDY, K. V. S. & PEI, D. C. T. 1969 Particle dynamics in solids–gas flow in a pipe. *Ind. Engng Chem. Fundam.* **8,** 490–497.

RIZK, M. A. & ELGHOBASHI, S. E. 1985 A mathematical model for a turbulent gas–solid suspension flow in a vertical pipe. Presented at the *5th Symp. on Turbulent Shear Flows*, Cornell Univ., Ithaca, N.Y.

RIZK, M. A. & ELGHOBASHI, S. E. 1989 A two-equation model for dispersed dilute confined two-phase flows. *Int. J. Multiphase Flow* **15,** 119–133.

ROGERS, C. B. 1989 The interaction between dispersed particles and fluid turbulence in a flat-plate boundary layer in air. Ph.D. Thesis, Stanford Univ., Calif.

RUBINOW, S. I. & KELLER, J. B. 1961 The transverse force on a spinning sphere moving in a viscous fluid. *J. Fluid Mech.* **11,** 447–459.

STAFFMAN, P. G. 1965 The lift on a small sphere in a slow shear flow *J. Fluid Mech.* **22,** 385–400.

SNYDER, W. H. & LUMLEY, J. L. 1971 Some measurements of particle velocity autocorrelation functions in a turbulent flow. *J. Fluid Mech.* **48,** 41–71.

SOO, S. L., IHRIG, H. K. & EL KOUH, A. F. 1960 Experimental determination of statistical properties of two-phase turbulent motion. *J. bas. Engng* 609–619.

SQUIRES, K. D. & EATON, J. K. 1989 Study of the effects of particle loading on homogeneous turbulence using direct numerical simulation. Presented at the *Int. Symp. on Turbulence Modification in Dispersed Multiphase Flows*, San Diego, Calif.

STEIMKE, J. L. & DUKLER, A. E. 1983 Laser Doppler velocimeter measurements of aerosols in turbulent pipe flow. *Int. J. Multiphase Flow* **9,** 751–754.

STOKES, G. G. 1851 On the effect of internal friction on the motion of pendulums. *Trans. Camb. phil. Soc.* **9,** 8–106.

TOROBIN, L. B. & GAUVIN, W. H. 1960 Fundamental aspects of solids–gas flow. Part V: the effects of fluid turbulence on the particle drag coefficient. *Can. J. chem. Engng* **38,** 189–200.

TSUJI, Y. & MORIKAWA, Y. 1982 LDV measurements of an air–solid two-phase flow in a horizontal pipe. *J. Fluid Mech.* **120,** 385–409.

TSUJI, Y., MORIKAWA Y. & SHIOMI, H. 1984 LDV measurements of an air–solid two-phase flow in a vertical pipe. *J. Fluid Mech.* **139,** 417–434.

WELLS, M. R. & STOCK, D. E. 1983 The effects of crossing trajectories on the dispersion of particles in a turbulent flow. *J. Fluid Mech.* **136,** 31–62.

YUDINE, M. I. 1959 Physical considerations on heavy-particle diffusion. *Adv. Geophys.* **6,** 185–191.